Journal of Thermal Analysis and Calorimetry (2023) 148:13775–13790
https://doi.org/10.1007/s10973-023-12595-2

Effect of different tube sizes on heat transfer characteristics of functionalized GNP and metal oxide nanofluids in conduit flow heat exchanger

K. H. Solangi[1,2] · T. A. Larik[1] · I. A. Memon[1] · A. A. Abro[1] · S. N. Kazi[2]

Received: 27 March 2023 / Accepted: 16 September 2023 / Published online: 19 October 2023

Abstract

This study demonstrates the enhanced heat transfer characteristics of functionalized propylene glycol-treated graphene nanoplatelets (FPG-Water), trimethylolpropane tris [poly(propylene glycol), amine terminated] ether-treated graphene nanoplatelets (FTM-Water), Al_2O_3 and SiO_2 nanofluids. Test sections made of stainless steel 316 circular tubes with different diameters (2 mm, 4 mm and 15 mm) were used at a consistent bar of heat flux 23,870 W m^{-2}. A covalent functionalization technique was used for developing exceedingly scattered FPG-Water- and FTM-Water-based nanofluids. The recorded thermo-physical properties of all the samples showed remarkable performance. By inspecting the size effect, the 2-mm-diameter test section showed highest heat transfer coefficient up to 116.4% in FPG-Water at 0.1mass% compared to base fluid. In 4-mm- and 15-mm-diameter test sections the highest heat transfer coefficient was detected to 100.6% and 91.7%. Moreover, Al_2O_3 and SiO_2 nanofluids exhibited decent enrichment in the heat transferal coefficients of up to 32.2% and 34.6% correspondingly. Besides, friction factor and Nusselt number showed a good degree of enhancement in all tested nanofluids. These findings give significant insight into the fluid flow and heat transfer properties of conduit flow heat exchangers, as well as perspective pathways for increasing thermal performance. The heat transfer coefficient and friction factor of FPG-Water and FTM-Water nanofluids obtained in this paper can contribute to design the advanced level heat exchangers for industrial purpose.

Keywords Nanofluids · Heat transfer · Stainless steel · Nusselt number · Functionalization

List of symbols

C_p	Specific heat (J g^{-1} K^{-1})
D	Diameter (m)
h	Heat transfer coefficient (W m^{-2} K^{-1})
K	Thermal conductivity (W m^{-1} K^{-1})
L	Tube length (m)
m^o	Mass flow rate (kg s^{-1})
Nu	Nusselt number
Pr	Prandtl number
q	Heat flux (W m^{-2})
Q	Heat transfer rate (W)
Re	Reynolds number
T	Temperature (°C)
U	Velocity (m s^{-1})
A	Cross section of the tube (m^2)
f	Friction factor
n	Number of tube passes
G	Mass velocity ([kg m^{-2} s^{-1})
W	Pumping power

Greek symbols

ρ	Density (kg m^{-3})
μ	Viscosity (Pa.s)
ε	Performance index
Δp	Pressure drop (Pa)
η	Efficiency of loop

Subscripts

bf	Base fluid
nf	Nanofluid
p	Particles
w	Tube wall
in	Inlet
out	Outlet

✉ K. H. Solangi
solangi.quest@gmail.com

1 Department of Mechanical Engineering, Faculty of Engineering, Quaid-e-Awam University of Engineering Science and Technology Nawabshah, Sindh, Pakistan

2 Department of Mechanical Engineering, Faculty of Engineering, University of Malaya, Kuala Lumpur, Malaysia

b Bulk fluid
ID Inner diameter
Tb Bulk temperature
OD Outer diameter

Introduction

The improvement of convective heat transfer and the associated investigational and theoretical investigation become an autonomous, significant and quickly emerging area of heat transfer theory [1]. Large heat loads are stifling the growth of many sectors such as fabrication, transfer, manufacturing and microelectronics [2, 3]. Therefore, the development of outrageous application of heat transferal setup has become the crucial primacy for the productions. There are several methods to raise heat transferal level. The heat transfer coefficient (HTC) is an essential factor that influences heat transferal amount. Heat transfer coefficient is distressed by heat exchanger geometrical elements like duct positioning, pitch, duct diameter and so on. According to the literature, heat transfer characteristics of various heat exchangers (such as casing and duct, helically coiled, straight tubular, elliptical hose, plate and structure) vary while even operating under the same circumstances [2, 4]. Heat transfer coefficient could also be improved by expanding fluid speed to a specific degree or by boosting the fluid's thermo-physical qualities such as viscidity, concentration and thermal conductivity [5, 6].

Several researchers have studied the thermo-physical and heat transferal features of metal oxide nanofluids [7–14]. Masuda et al. [15] scientifically checked the thermal conductivity of Al_2O_3–water nanofluids about 32.4% increasing for 4.3% volume fraction nanoparticle charging. Young hwan et al. [16] deliberate alumina–water nanofluids which shows about 8% betterment in thermal conductivity and approximately 20% augmentation in convective heat transferal coefficient with 3% volume density. Similarly, Abdolbaki et al. [17] calculated the thermal conductivity of SiO_2 nanoparticles in base fluids such as bioglycol (BG)/water 20:80%. The highest thermal conductivity development was observed about 7.2% in the 2vol% at a temperature of 70 °C. A number of studies have shown that the nanofluids' thermal conductivity increases with a rise in density and decreases with an increase in temperatures [2, 18]. Further, Minakov et al. [1] worked on the turbulent forced convection of SiO_2 and Al_2O_3 nanofluids. They used the stainless steel tube as a test section with 6 mm in diameter. They obtained that, with rising nanoparticles absorption, the local and average heat transferal coefficients at a stable Reynolds number rise. Investigational calculation of convective heat transferal coefficient of nanofluids running through a duct has been recorded by many scholars, who have deliberated various kinds of metal oxide nanoparticles [19–23]. In the present study, along with metal oxide nanofluids, graphene-based nanofluids have also been considered.

Several studies have come out recently about how nanomaterials made of carbon can be used to make nanofluids [24–29]. Muhammad et al. [30] investigated heat transfer characteristics and frictional loss for fully developed turbulent flow of graphene nanoplatelet through a stainless steel duct. It was found that the convective HTC of the aforementioned GNP nanofluid was roughly 83–200% and that an increase in pressure drop of up to 14.7% may be achieved very instantly. With the addition of graphene nanoplatelets to water–ethylene glycol blends, the convective heat transfer coefficient and pressure drop were measured and reported by Selvam et al. [29]. Sodium deoxycholate as the surfactant was employed to make durable nanofluid dispersals, and the assessment component was prepared of glowing annealed hardened copper conduit. The maximum HTC increased up to 170% with 0.5 vol% of graphene loading was obtained. Further, the pressure fall with reverence to GNP packing for the equal mass flow rate of nanofluid was up to ~ 15% simply. Hooman et al. [24] studied the convective heat transfer as well as the pressure drop of water-based nanofluids with functionalized graphene nanoplatelets in a square heated duct. The simplistic technique was employed for the formation of functionalized GNP nanofluids. The highest improvement in HTC was 19.68% with 9.22% increase in friction factor for the load density of 0.1% at a Reynolds number of 17,500. Similarly, Emad et al. [31] inspected the heat transferal augmentation for GNP nanofluids in turbulent stream conditions. As the test section, a straight piece of stainless steel pipe with a length of 1400 mm and 12mm was used. They found that along with enhancement in physical properties the Nusselt number (Nu) of the GNP nanofluid was greater than the base fluid by about 3–83% and the increase in the pressure drip ranged from 0.4 to 14.6%. In the literature, various research works have been done on thermal and rheological features of metal oxide- and carbon-based nanofluids. Conversely, to the best of writers' familiarity, there is no any work has been published yet which could explain the influence of dimension on the performance of convective heat transfer of nanofluids. However, heat transfer enhancement in graphene-based nanofluids and its synthesis is still in the considerations of the researchers, and so, many groups and organizations are doing research in the relevant areas. Sundaram et al. [32] used water- and graphene nanoplatelet-based nanofluid. They worked on its heat transfer behavior, synthesis and stability. They used 4 different concentrations (0.05, 0.5, 0.75 and 1 mass%), they observed the significant change in decrease in density by 8.5% to 15% for 1 mass%, and the melting duration was reduced by 33% by adding 0.5 mass% of GNP. Sabastian et al. [33] found that the heat transfer coefficient of GNP nanofluids was superior to that of multiwalled carbon nanotubes nanofluids up to 26% which is significant. Esmaeilzadeh et al. [34] studied the functionalized graphene nanofluid to investigate the heat transfer characteristics in a sintered wick heat pipe. The maximum enhancement in thermal conductivity was achieved up to 40%. Also they found that tilt angle of heat pipe has a substantial impact on the thermal properties, and performance is increased by 79%. Therefore, they found that heat pipe thermal resistance was reduced using GNP nanofluids. Simultaneously, Chenlei et al. [35] used Fe_3O_4/graphene nanofluid with different concentrations in microchannel heat sink. They observed that the selected nanofluids can significantly reduce the thermal resistance and pressure drop in the microchannel heat sink.

So, this study aims to investigate the effect of size variation in FPG-Water, FTM-Water, Al_2O_3 and SiO_2 water-based nanofluids on their heat transfer and friction reduction capabilities. To examine the size effect, a standard continuous test duct (test section) with a span of 1500 mm (internal diameters: 2, 4, 15mm and exterior diameters: 6, 8, 19 mm) was used as the test section. The convective heat transfer in rounded ducts of various diameters was recorded at stable wall heat flux of 23,870 W m^{-2}. This investigation was carried out within the Reynolds number range of 3,900 to 11,700. The study focused on investigating the effect of dispersed nanoparticle concentration on various key parameters such as thermal characteristics, convective heat transfer coefficient, Nusselt number and friction factor. The goal of this investigation is to explore the sizing effect on the convective heat transferal amount and friction deficit of the nanofluids, to functionalize the graphene-based nanofluids and to examine the thermo-physical characteristics of developed nanofluids.

Material and methods

Functionalization and development of FPG-Water, FTM-Water, Al_2O_3 and SiO_2 nanofluids

A superb graphene nanoplatelets (GNP) was procured from XG Sciences Firm, with a normal facing surface of 750 m^2 g^{-1} and a carbon content of above 95%. Sigma-Aldrich supplied all further chemicals.

GNP is initially covalently functionalized with carboxyl clusters for the synthesis of FPG-Water. Pristine GNP is sonicated for 12 h at 60 °C with a 3:1 blend of H2SO4–HNO3 acids and to thrilling for 36 h at the identical temperature to generate carboxylated GNP (GNP-COOH). The solution was completely separated by centrifugation at 11,000 rpm with DI water, while the PH of the supernatant reaches about 4–5 instantaneously. The specimen is subsequently dried for 48 h at 50 °C inside the kiln. One gram of GNP-COOH and one hundred milliliters of propylene glycol were ultrasonically processed for ten minutes before 13.4 mL of H_2SO_4 were inserted gradually. The blend was sonicated for 8 h before being stirred for 12 h at 70 °C on a magnetic stirrer. In accordance with the principle of equilibrium, the water generated during the Fischer esterification process is eliminated via evaporation to accelerate the operation. For better understanding, Fig. 1 shows the preparation method of functionalized FPG-Water and FTM-Water nanofluids for this study. The equilibrium could be changed by taking the water product out of the reaction system and shifting it to the right side. In the presence of an acid, an ester could potentially be produced through the reaction between a carboxylic acid and an alcohol. After being cleansed with ethanol and THF, this solution was spun up around 11,000 rpm with anhydrous to confiscate some unreacted substances. The sample was subsequently kept inside the kiln for 48 h at a temperature of 60 °C.

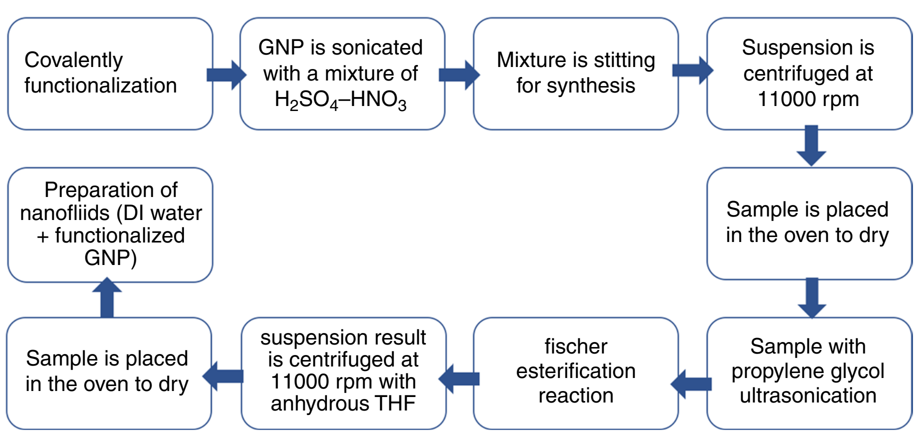

Fig. 1 Preparation method of functionalized FPG-Water and FTM-Water nanofluids

Similarly, for the preparation of FTM-Water the process is similar as for FPG-Water, only in FTM-Water situation after centrifuge when the pH come out at 3–4; after that, the model spends around 4 days at 500 degrees in the kiln drying overnight. Hence, 1 g of GNP-COOH was sonicated for 10 min in 100 mL of trimethylolpropane tris[poly(propylene glycol), amine terminated] ether-treated graphene nanoplatelets, followed by the progressive addition of 13.4 milliliters of H_2So_4. The nanofluids are being produced utilizing a two-step procedure that involves dissolving dry aluminum oxide and silicon dioxide (Al_2O_3 nanopowder with a particulate size of 50 nm and SiO_2 nanopowder with a particulate size of 50 nm, respectively) into desalinated water. Ultrasonication was applied for 60 min to break up huge assortments and achieve uniform distribution of nanoparticles.

Fig. 3 Various test segments of stainless steel grade 316 with different diameters (2mm, 4mm and 5mm)

Experimental setup

The experimental layout and schematic diagram for the present investigation are shown in Fig. 2, which contains a flowing hoop, warmed testing units, chilling segment, gauging apparatuses, data gathering and controller. Chilling segment is a refrigerated bath circulator (DAIHAN brand, WCR-P30) and was used to balance the heat input and it is inside the jacketed tank. This refrigerated bath has RS232C interface for remote monitoring and controlling with computer. Moreover, it has powerful circulation pump which ensures temperature uniformity. Electromagnetic flow meter (model N-FLO-25) was used to measure fluid flow rate. A magnetic flow meter (mag flowmeter) is a volumetric flow meter which does not have any moving parts and is ideal for wastewater applications or any dirty liquid which is conductive or water based. The operation of a magnetic flow meter or mag meter is based upon Faraday's law, which states that the voltage induced across any conductor as it moves right angles through a magnetic field is proportional to velocity of that conductor. Differential pressure transducer (model IDP10-T22D21D-LIT) with accuracy of ± 0.075% of span connected to the inlet and outlet of the test section was used in this experimental setup. A SIMATIC WinCC control and acquisition system was used to control power supply and to record the data which was connected with the SCADA system. The maximum power output of 20A and output voltage of 0 ~ 260 V was used to regulate the voltage.

This setup makes a considerably more accurate representation of actual engineering application by closely resembling heat transfer in most heat exchangers. All components of the assessment system and the experimental method are elucidated in detail in the auxiliary data. Moreover, for examining the size influence, a straight continuous stainless steel 316 tubes with a span of 1500mm was used as test section. The inner diameter of the test sections was 2mm, 4mm and 15mm, and the outer diameter was 4mm, 8mm and 19mm. These three different test sections of different diameters have been selected to compare the heat transfer performance at different surface areas that how it attributes.

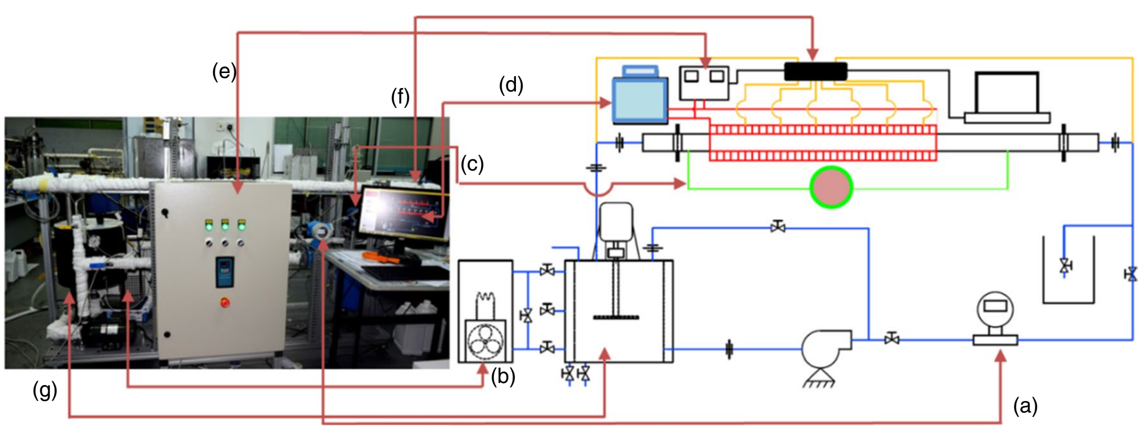

Fig. 2 Pictorial and schematic representation of the experimental setup along with its major components: **a** flow meter, **b** cooling unit, **c** differential pressure transmitter, **d** auto transformer (variac), **e** multifunction meter, **f** data acquisition unit and **g** reservoir tank

Furthermore, Fig. 3 illustrates the three dissimilar test sections of identical material with altered diameters. The reason to select the three different sizes of the test sections was to compare the thermo-physical properties as well as heat transfer effect on each size due to different circumstances during the flow in the tubes.

In this investigation, the thermo-physical properties of nanofluids at concentrations of 0.1mass% were tested (Table 1). Thermal conductivity of 0.1mass% samples was measured using the KD2 Pro thermal conductivity equipment, which utilizes the transient hot chord technique. The accuracy of the KD2 Pro is given as 5% by the manufacturer over a span of temperatures from 0 to 60 °C [36]. However, it is found, through trial and error, that the KD2 Pro operates very accurately if the probe is setup perfectly vertical and an isothermal bath is used to maintain the sample at 25 °C. These techniques prevent convection problems and the external boundary effect problems as well. The measurements were taken over a temperature range of 25–50°C. Figure 4 shows how the thermal conductivity of FPG-Water, GNP-water, FTM-Water, Al_2O_3 and SiO_2 nanofluids which changes with increase in temperature. The thermal conductivity of FPG-Water and FTM-Water increases more noticeably with increase in temperature. As a consequence of this, it has been demonstrated that temperature has a substantial effect on the thermal conductivity of all prepared nanofluids.

Strength of the created nanofluids was measured by UV–photospectrometer up to 35 days. A UV–Vis spectrum is a common procedure employed to study dispersibility of aqueous suspensions with sedimentation time. This procedure works based on various light wavelengths in which it could be absorbed or distributed by other substances in the nanofluids. The UV–Vis spectra procedure follows the Beer–Lambert law and shows the absorbance is directly proportional to the nanoparticle concentration in colloids. Although the stability of nanofluid is very important in order for practical application, the data are limited for estimating the stability of nanofluids. The light transmission of all samples were measured with a Shimadzu UV spectrometer (UV-1800) operating between 190 and 1100 nm. The nanofluid solution was diluted with distilled water to allow sufficient transmission while each measurement was repeated three times to achieve a better accuracy [37].

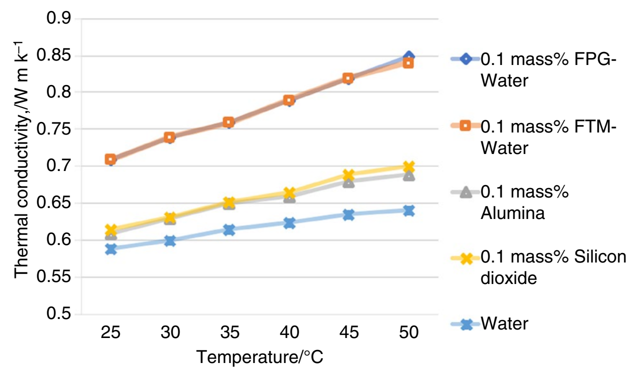

Fig. 4 Thermal conductivity of selected nanofluids as a function of hotness

All functionalized and metal oxide nanofluids showed good degree of dispersion and higher stability up to 90% even after one month. It is observed that the colloidal blend exhibited a steady decrease in relative concentration over time. This specifies the particle concentration level, and therefore, strength has decreased and remarkably less than 10% deposit.

Data processing

The objective of this research was to analyze the convective heat transfer features and power handling capabilities of various nanofluids, including FPG-Water, FTM-Water, Al_2O_3 and SiO_2 nanofluids. In order to determine heat transfer and hydrodynamic performance in sealed hose heat transferal evaluation, computations of computable data were processed in accordance with comparable guidelines as specified earlier. Table 2 provides analytical representations of heat transfer characteristics such heat flux, heat transfer coefficient, Nusselt number, friction factor, Reynolds number and Prandtl number.

Table 1 Specific heat, dynamic viscidness and density of the nominated nanofluids

Nanofluids	Density/kg m^{-3}	Specific heat/J kg^{-1} K^{-1}	Viscidness/Pa-s
FPG-Water	1055.863	2807.352	0.003129
FTM-Water water	1055.863	2807.352	0.003130
Al_2O_3	1072.747	3039.524	0.002155
SiO_2	1057.886	2796.342	0.003001

Table 2 Factors to analyze heat transferal and hydrodynamic performance in heat transfer investigation

Parameter	Units	Symbol	Expression
Heat flux	W m^{-2}	`	$\frac{VI}{\pi DL}$
Prandtl number	–	Pr	$\frac{\mu C_p}{k}$
Reynolds number	–	Re	$\frac{\rho VD}{\mu}$
Nusselt number	–	Nu	$\frac{hD}{k}$
Heat transferal constant	W m^{-2} K^{-1}	h	$\frac{q'}{T_w - T_b}$
Friction factor	–	f	$\frac{\Delta P}{(L/D)(\rho V^2/2)}$

Results and discussions

Functionalization analysis of FPG-Water and FTM-Water nanofluids

In a previous work, the FTIR spectra of pure GNP, FPG-Water and FTM-Water were characterized [4, 28]. As compared to unspoiled GNP, the functionalized GNPs tasters showed clear indications of different functionalities clusters. The complete index of summits and their explanations are found in [4, 28]. The PG (propylene glycol) was functionalized when O–H, COO stretching and CH2 bending vibrations peaked at 3403 cm^{-1}, 1453 cm^{-1} and 1385 cm^{-1}, respectively [28]. As a result, the existence of peaks at 3430 cm-1 for OH and NH extending vibrations of primary amine/symmetrical NH extending vibes completing FTM-Water functionalization [4].

Furthermore, Raman spectrum analysis of the FPG, FTM and pure GNP is addressed in our previous research [4, 28]. The Raman spectra of all specimens were examined, and the presence of D and G bands was observed. Specifically, the D band was detected at approximately 1362 cm^{-1}, while the G band was detected at approximately 1592 cm^{-1}. Amorphous/disordered carbon (sp3) is associated with the D bands, whereas graphitic carbon (G bands) is connected with the sp2 hybridization (sp2). Covalent functionalization converted more sp2 hybridized carbons to sp3 hybridized carbons, as shown by an increase in the ID/IG ratio. Yet, it is clear that FPG and FTM tasters had a larger strength percentage than the pure GNP.

Figure 5 depicts TEM and SEM pictures of virgin GNP and FPG. Though TEM as well as SEM imageries are incapable of identifying small functional groups, they can indicate surface deterioration and rumples in GNPs generated via PG functionalization. In general, particular multilayer GNP splinters with appropriate and high grain size can be examined in the portrait. The FPG sheets kept their shape and size, as seen by the outcomes of the TEM and SEM. Significant morphological and surface deterioration alterations might be detected in the TEM and SEM photographs. The crinkles on the GNP facet that can be observed in the TEM photos are caused by the fact that the 2D structures are extremely fragile. The existence of these motifs in FPG could be attributable to the production of crinkles (ripples) during sonication as a result of the flexibility of his GNP flakes after treatment.

Similarly, Fig. 6 demonstrates the TEM picture of FTM. The image can depict the GNPs' surface deterioration and ripples that resulted during FTM-Water functionalization. In general, certain GNP sheets with significant particle sizes may be grasped. The figure demonstrates that the FTM films retained their figure. In addition, streaks visible in the TEM portraits are crinkles on the GNP face caused by the 2D structure's intrinsic variability. The fact that these streaks showed up in FTM could have been caused by ripples that formed during the sonication process because the GNP splinters were more flexible after the treatments. It is important to note that functionalization can improve crinkles by making the surfaces more wettable.

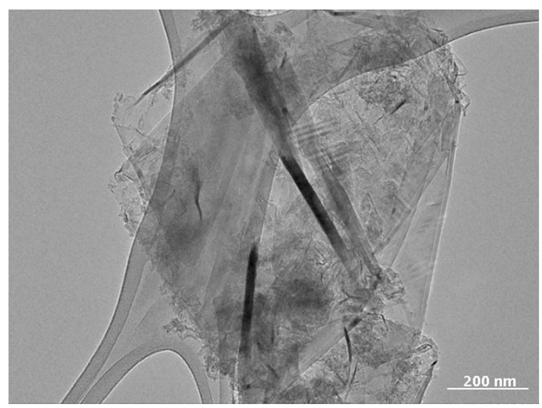

Fig. 6 TEM image of FTM

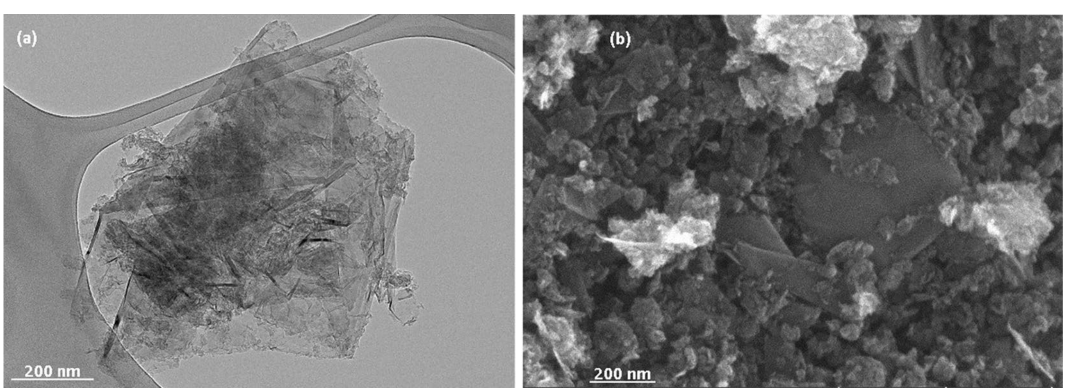

Fig. 5 **a** TEM and **b** SEM portraits of FPG

Characterization of Al_2O_3 and SiO_2

Figure 7 displays the TEM images of Al_2O_3/water nanofluids with different magnifications. The alumina nanoparticles may be seen to be rectangular and rodlike in structure (view Fig. 7 a and b). Figure 7 (c and d) indicates, however, that samples containing 0.1mass% dispersant have very little conglomeration and achieve excellent suspension. Al_2O_3 nanofluids were sonicated up to 60 min. Al_2O_3 nanofluids were sonicated for up to 60 min in order to obtain the best dispersion. It is observable that all components are smaller than 50 nm in size and are the same size. To obtain greater thermal conductivity, Al_2O_3 nanofluids were created without surfactant. Figure 8 (a and b) exhibits TEM pictures of silica nanoparticles that are rounded and rodlike form. However, Fig. 8 (c and d) reveals that the specimen has a very lower assortment and has touched the superior suspension. It is really observed that all constituents are of equal in size and are less than 50nm in size. To attain the steady dispersion, nanofluids were sonicated up to 60 min. Also like Al_2O_3 to attain the greater thermal conductivity no any surfactants was employed for SiO_2. The bulk of the SiO_2 and Al_2O_3 samples is of excellent purity, lending credibility to the synthesis process prescribed earlier.

The zeta potential and particle size variations of Al_2O_3 and SiO_2 nanofluids are illustrated in Table 3. The dynamic light scattering (DLS) technique is used to examine variations in particle size distribution in order to validate the aggregate size of nanofluids in DI water. To conduct the DLS evaluation, the samples were carefully transported to a folded capillary cell featuring gold-plated electrodes and constructed from polycarbonate. Particle size distribution analysis was performed using a Zetasizer Nano instrument from Malvern Instruments Ltd., UK, with the temperature set at 25 °C. First, at the utmost concentration of 0.1 mass%, Al_2O_3 does not exhibit significant aggregation or coagulation. The Al_2O_3 nanofluids' particle size scattering indicates that the hydrodynamic size has consistently increased. This explains the development of tiny aggregates, which are compatible with UV–Vis data. At a maximum concentration of 0.1 mass%, Al_2O_3 exhibits excellent dispersion and coagulation. As per the principle of stabilization, a larger magnitude of zeta potential leads to increased electrostatic repulsion between particles, thereby enhancing the stability of the mixture. When particles possess a high surface charge, their tendency to aggregate is impeded due to the antagonistic nature of the contacts between them. This electrostatic

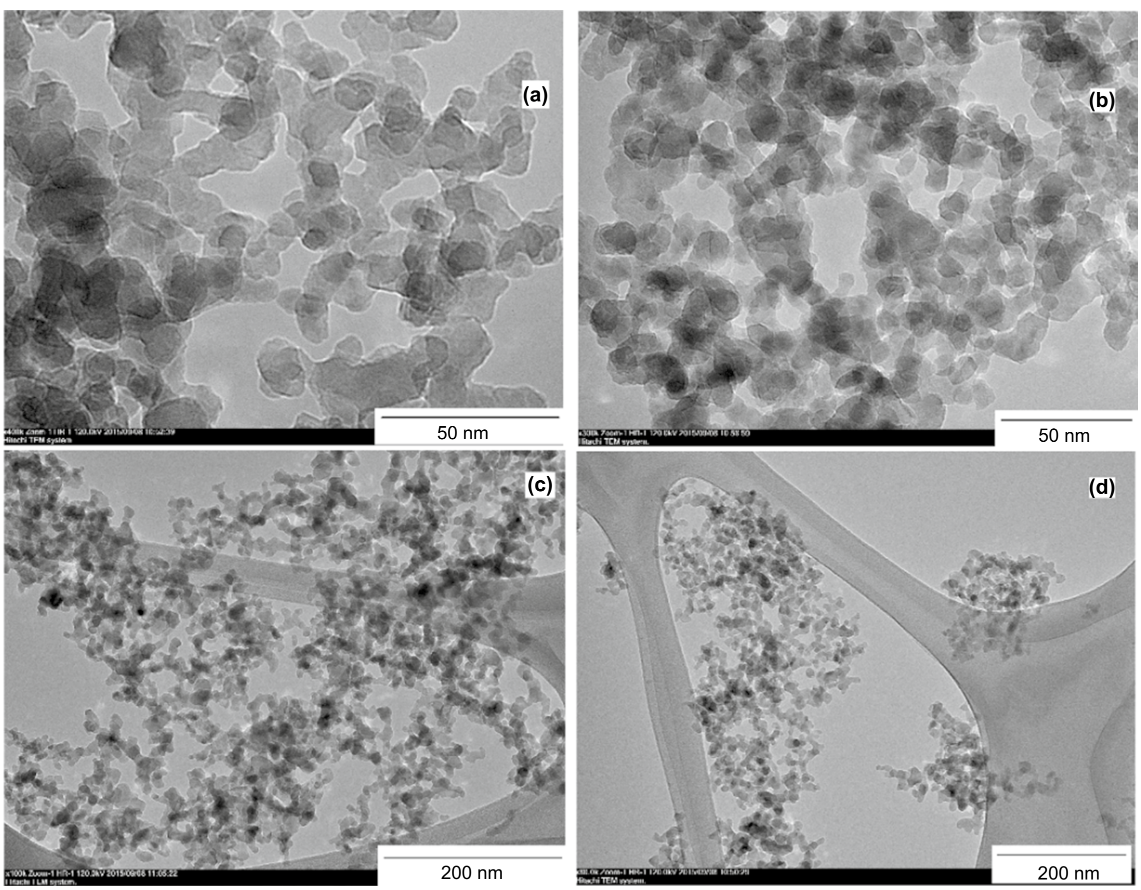

Fig. 7 TEM portraits of Al_2O_3 nanoparticles at 0.1mass%

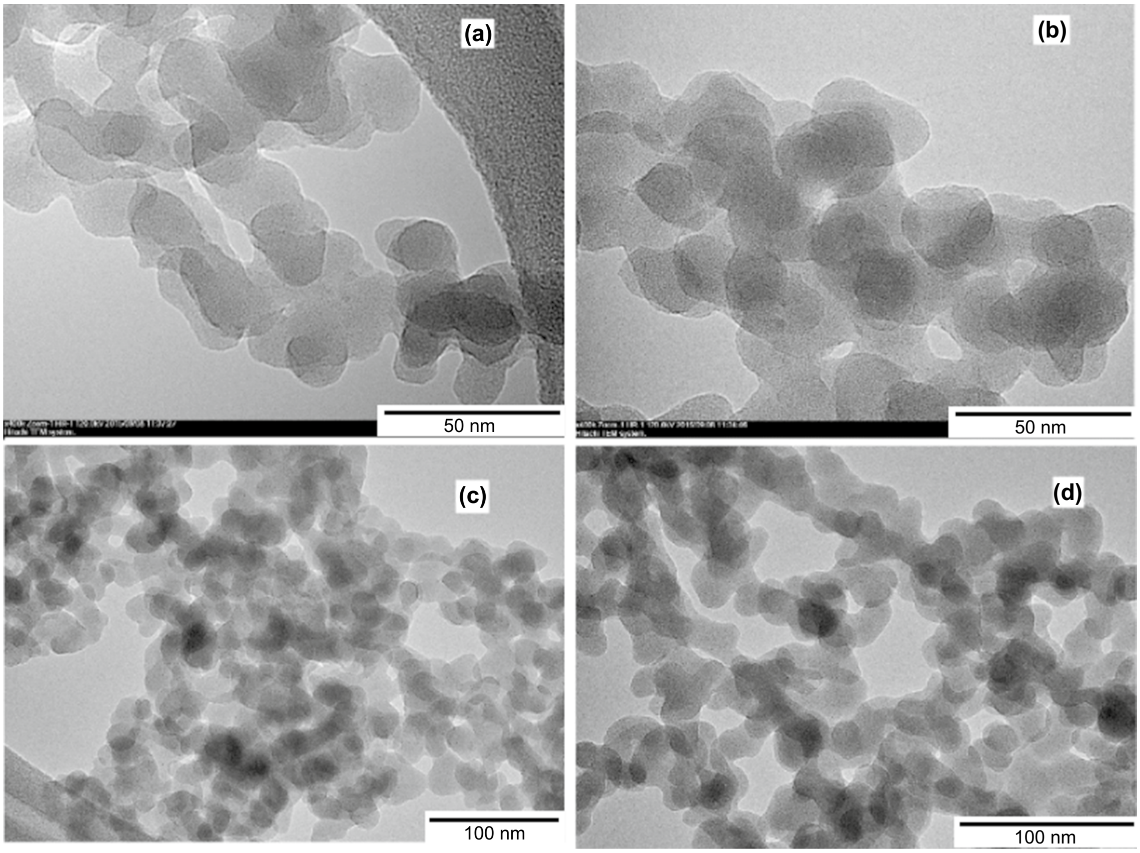

Fig. 8 TEM portraits of SiO_2 nanoparticles at 0.1mass%

Table 3 Zeta potential, average particle size spreading, mobility and polydispersity index (PDI) of Al_2O_3 and SiO_2 in distilled water

No	Sample	Time/Day	Average particle size distributions/nm	Polydispersity index (PDI)	Zeta potential/mV	Mobility/ µm cm Vs^{-1}
1	Al_2O_3	7	138.2	0.192	50.1	3.93
2	SiO_2	7	207.9	0.274	− 35.4	− 2.776

repulsion provides a barrier to the frequent clumping of particles, thereby improving their dispersion in the nanofluid.

Al_2O_3 and SiO_2 zeta potential and polydispersity index (PDI) levels at neutral pH are listed in Table 3. The results presented in Table 3 suggest that a higher zeta potential (either positive or negative) is necessary for effective electrostatic repulsion between the particles. After 1 h of sonication, it is noticeable that Al_2O_3 displays a considerably higher positive charge of approximately + 50 mV after 7 days. After 7 days at 25 °C, the zeta potential implications of SiO_2 reveal a reasonable level of stability. In fact, the zeta potential progressively fluctuates throughout a 7-day period, although it stays mostly steady over time. Nanofluids that possess a zeta potential exceeding + 30 mV or falling below -30 mV exhibit excellent stability [38]. The experimental results suggest that the electrostatic interaction between metal oxides is strong enough to overcome the grain attraction.

Uncertainty analysis of the test results and accuracy of the applied instruments

Uncertainty analysis of the relevant parameters and the measured data obtained from the data reduction process is presented in Table 4 and is estimated based on the error propagation method. Furthermore, the accuracy of the applied instruments which are used in this study is given in Table 5.

Effect of size on heat transfer coefficient and Nusselt number

In the first stage of the experiment, a stainless steel test bench with a 2 mm diameter was utilized to assess a heat flux of 23,870 W m^{-2}. The objective of this stage was to investigate the impact of FPG-Water, FTM-Water, Al_2O_3 and SiO_2 nanofluids, all with a mass concentration of 0.1 mass%, on the convective heat transfer coefficient and Nusselt number. Figure 9 specifies the convective heat transfer coefficient of entirely nominated nanofluids. The results demonstrate the dependence of the heat transferal coefficient on nanofluid concentration at flow velocities between 1 and 3 m s^{-1}. Investigational findings noticeably reveal a virtuous amount of improvement in the convective heat transfer coefficient, and this augmentation rises as the speed increases. It is discovered that increasing the convective heat transfer coefficient of nanofluids beat increasing thermal conductivity at certain mass concentrations. The convective heat transfer coefficient goes up as the speed of all nanofluids goes up. According to the findings, both nanofluids exhibit higher heat transfer efficacy compared to desalinated water. Notably, FPG-Water, FTM-Water, Al_2O_3 and SiO_2 nanofluids demonstrated the highest variation in heat transfer coefficient at a heat flux of 23,870 W m^{-2}, with values of 116.4%, 109.7%, 32.2% and 34.6%, respectively, in a 2-mm-diameter experimental section. This extensive development is attained by attaching a very lesser quantity of nanoparticles to the distilled water.

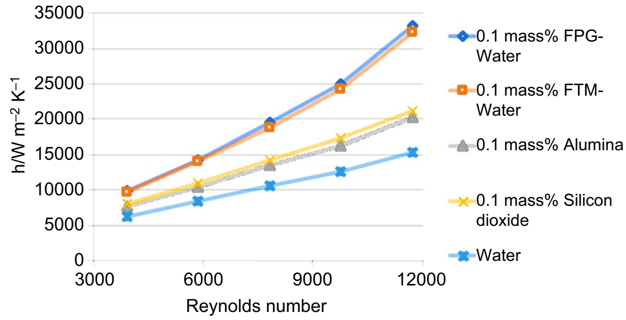

Fig. 9 Convective heat transfer coefficient of whole nanofluids in 2 mm test rig at inlet temperature of 30 °C at input power of 23,870 W m^{-2}

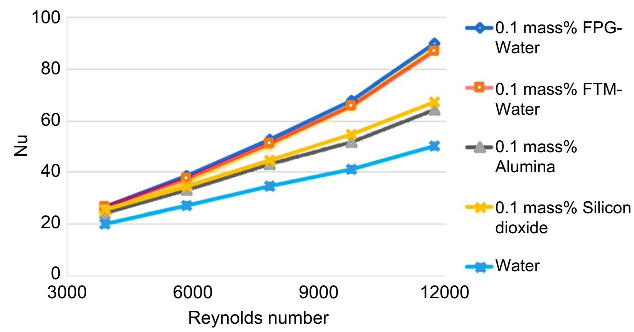

Fig. 10 Enhancement in Nusselt number of tested nanofluids at various Re with input power of 23,870 W m^{-2} (2 mm test section)

In Fig. 10, the average Nusselt number of FPG-Water, FTM-Water, Al_2O_3 and SiO_2 nanofluids is plotted against the Reynolds number at a constant heat flux of 23,870 W m^{-2}. The purpose of this analysis is to evaluate the convective-to-conductive heat transfer ratio of the nanofluids. The experimental results revealed that the average Nusselt number of FPG-Water, FTM-Water, Al_2O_3 and SiO_2 nanofluids increased significantly. These results imply that the size and movement of the nanoparticles within the nanofluids play a pivotal role in the Nusselt number. At the specific

Table 4 Uncertainty ranges of the parameters used in the present study

Variable name	Uncertainty range/%
Nu, avg	± 10
Nu, Local	± 8
h, avg	± 6
h, local	± 9
f	± 10

Table 5 Accuracy of applied instruments used in the present work

Instruments	Accuracy range
KD2 Pro (thermal property analyzer)	± 5% (temperatures from 0 to 60 °C)
Differential scanning calorimetry (DSC) (Mettler Toledo 82 °C)	Error ± 0.25
UV spectrometer (UV-1800)	Wavelength accuracy ± 0.3 nm (for entire range), photometric accuracy ± 0.002 Abs at 0.5 Abs
Hoffman Muller inverter	Speed control accuracy ± 0.2% (sensorless vector control)
N-FLO-25 Electromagnetic flow meter	Measurement accuracy ± 0.5%
Differential pressure transducer (model IDP10-T22D21D-LIT)	Accuracy of ± 0.075%
Cooling unit (DAIHAN brand, WCR-P30)	Temp. range and accuracy − 25 °C ~ + 150 °C, ± 0.1 °C

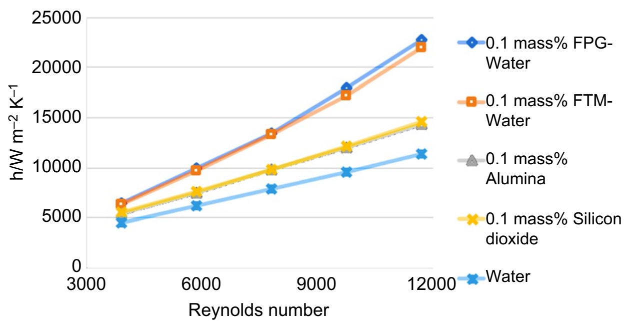

Fig. 11 Convective heat transfer coefficient of all nanofluids in 4 mm test rig at inlet temperature of 30 °C at input power of 23,870 W m^{-2}

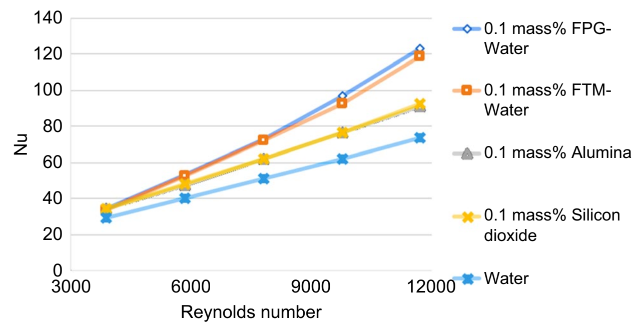

Fig. 12 Enhancement in Nusselt number of tested nanofluids at various Re with input power of 23,870 W m^{-2} (4 mm test section)

combination of a Reynolds number of 11,770 and a heat flow of 23,870 W m^{-2}, the maximum average Nusselt number achieved was at 0.1% by mass, as confirmed by a corresponding value of Nu = 11,770. Enhancing the thermal conductivity of the working fluid can lead to a decrease in the temperature difference between the tube wall and the bulk fluid in the confined conduit, which in turn can result in a higher Nusselt number for the nanofluid. At a heat flow of 23,870 W m^{-2}, it was observed that the Nusselt number increased by 79% for FPG water, 74% for FTM-Water, 26.4% for Al_2O_3 and 26.4% for SiO_2.

Convective heat transferal constants of 0.1 mass% FPG-Water, FTM-Water, Al_2O_3 and SiO_2 nanofluids were measured in a 4-mm-diameter apparatus under a heat flow of 23,870 W m^{-2}. Figure 11 depicts the convective heat transfer coefficients of all approved nanofluids. It illustrates the heat transfer coefficient in relation to the nanofluid concentration at flow rates between 1 and 3 m s^{-1}. The investigational outcomes noticeably express a virtuous level of improvement in the convective heat transfer coefficient, and this development rises as the speed goes up. At different mass concentrations, the changes in the convective heat transferal parameter of nanofluids are much greater than the changes in their thermal conductivity. The convective heat transfer factor rises with increasing velocity for all nanofluids, suggesting that both nanofluids have more heat transfer potential than pure water. In an experimental setting with a diameter of 4 mm and a heat flow of 23,870 W m^{-2}, the nanofluids with the highest increases in heat transfer coefficient were FPG-Water (100.68%), FTM-Water (93.25%), Al_2O_3 (26.45%) and SiO_2 (31.25%), in that order. FPG-Water showed the maximum gain, followed by FTM-Water (93.25%), FTM-Water (93.25%). This significant improvement is achieved by dispersing a vanishingly small number of nanoparticles throughout the purified water. Through correlating the results of a 4 mm test segment with those of a 2 mm experiment setup, the heat transfer coefficient consequences are barely lesser in 4 mm experiment setup due to superior diameter size.

Figure 12 offers a fascinating insight into the convective and conductive heat transfer ratios of FPG-Water, FTM-Water, Al_2O_3 and SiO_2 nanofluids. The figure illustrates the Nusselt number of these nanofluids as a function of the Reynolds number, providing valuable information on their heat transfer capabilities at a heat flux of 23,870 W m^{-2}. The Nusselt numbers for all the tested substances, such as FPG-Water, FTM-Water, Al_2O_3 and SiO_2, were found to be higher. FTM-Water, Al_2O_3, SiO_2 and FPG-Water nanofluids were investigated to see how material and motion affected the Nusselt number. The overall peak Nusselt number was determined to be 0.1 mass percent with Re = 11,770 and a heat flow of 23,870 W m^{-2}. When nanofluids have high Nusselt numbers, it means they have high thermal conductivity. This leads to lower temperatures and smaller differences in temperature between the tube wall and the bulk fluid in a closed channel. The Nusselt number rose by 66.7% in FPG-Water, 60.6% in FTM-Water, 23.4% in Al_2O_3 and 25% in SiO_2 when subjected to a heat flow of 23,870 W m^{-2}.

In a stainless steel test rig with a diameter of 15 mm and a heat flux of 23,870 W m^{-2}, the convective heat transfer coefficients of FPG-Water, FTM-Water, Al_2O_3 and SiO_2 nanofluids were scrutinized at a mass concentration of 0.1 mass%. The convective heat transfer coefficient of totally nominated nanofluids is presented in Fig. 13. At flow speeds ranging from 1 to 3 m s^{-1}, it reflects the heat transfer factor as a function of nanofluid concentration. The research's findings clearly show that the convective heat transfer coefficient has been improving at a significant rate, and this rate increases as the speed increases. It has been discovered that boosting the convective heat transferal constant of nanofluids surpasses increasing thermal conductivity over a wide range of mass concentrations. The convective heat transfer factor grew by raising the velocity in all nanofluids, indicating that both nanofluids have more heat transfer potential than plain water. In a 15-mm-diameter stainless steel test section at a heat flux of 23,870 W m^{-2} showed the highest increase in heat transfer coefficients for 0.1 mass% FPG-Water (91.7%), FTM-Water (85.7%), Al_2O_3 (24.25%) and SiO_2 (26.37%).

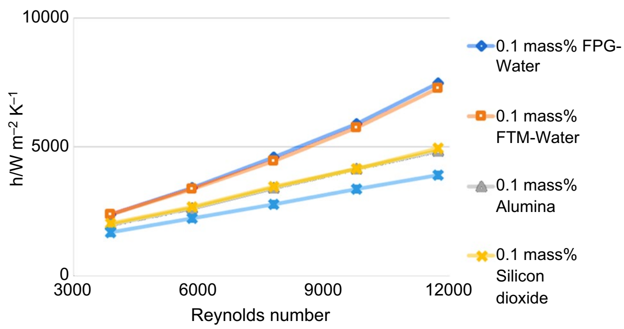

Fig. 13 Convective heat transfer coefficient of completely nanofluids in 15 mm test section at inlet temperature of 30 °C at input power of 23,870 W m^{-2}

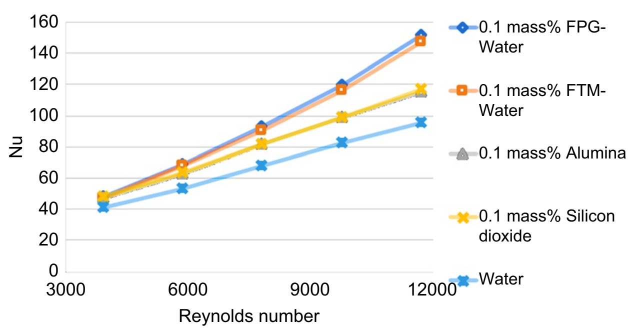

Fig. 14 Enhancement in Nusselt constant of tested nanofluids at various Re with input power of 23,870 W m^{-2} (15 mm test section)

This huge improvement is accomplished by introducing a little amount of nanoparticles into pure water. When the facts from the 15 mm stainless steel test section is compared to the data from the 4 mm and 2 mm stainless steel test units, the heat transfer coefficient results in the 15 mm stainless steel test unit are slightly lower.

Figure 14 presents the Nusselt number data for FPG-Water, FTM-Water, Al_2O_3 and SiO_2 nanofluids as a percentage of the Reynolds number at a heat flux of 23,870 W m^{-2}. This provides a quantitative analysis of the contribution of convective-to-conductive heat transfer. The results indicate that the average Nusselt number for all the nanofluids increased in each instance. The average Nusselt number of Al_2O_3, FPG-Water, FTM-Water and SiO_2 is influenced by the size and movement of the nanoparticles. The highest average Nusselt number was observed at 0.1% by mass, with a Reynolds number of 11,770 and a heat flux of 23,870 W m^{-2}. The increased thermal conductivity of the working fluid lowers the circulation temperature, resulting in a low temperature variance among the duct side and the bulk fluid in narrow conduits and a high Nusselt number. At 23,870 W m^{-2} heat flux, FPG-Water, FTM-Water, Al_2O_3 and SiO_2 experienced significant increases in Nusselt numbers, with

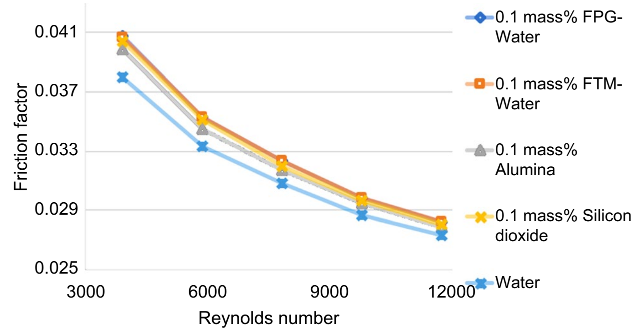

Fig. 15 Friction factor of tested nanofluids in 2-mm-diameter test section at altered velocities and input power of 23,870 W m^{-2}

the percentages being 59.3%, 54.4%, 21.3% and 22.9%, respectively.

Effect of size on friction factor

The frictional component of FPG-Water, FTM-Water, Al_2O_3 and SiO_2 nanofluids was recorded as they passed through a stainless steel test unit of 2 mm diameter under different circumstances and at different velocities (see Fig. 15). Although there are certain instabilities in the computed friction factor for different velocities, it was discovered that the friction parameter diminishes as the velocity of nanofluids rises. The maximum increase in friction parameter was up to 5.53% at speeds between 1 and 3 m s^{-1} at 0.1 mass% FPG-Water. The friction factor of FTM-Water was similar to FPG-Water. For metal oxides, the friction factor of Al_2O_3 rose to 3.87%, while SiO_2 rose to 5.33%, which is somewhat higher than Al_2O_3. It is clear that when velocity increases, the reliance of the friction parameter on the nanofluids reduces.

Friction parameters of all tested nanofluids in stainless steel test section of 4 mm diameter were also checked. It was detected that along with reduction in heat transfer coefficient in 4 mm test section compared to 2-mm-diameter test section the friction constant for entire substances similarly dwindled. The friction aspect of FPG-Water amplified up to 7%, and for FTM-Water, it augmented up to 6.9%. Likewise for Al_2O_3, the friction parameter amplified up to 4.74%, and for SiO_2, it raised 6.15, respectively (see Fig. 16).

Figure 17 shows the recorded friction coefficient of all substances in stainless 316 test section of 15 mm diameter. The friction element for FPG-Water rises to 7.61%. Similarly, the friction variable for FTM-Water nanofluids it amplified to 7.60%. Subsequently, for metal oxides, the friction variable for Al_2O_3 was found to be 5.91%, whereas the friction parameter of Al_2O_3 rose to 6.70 as a result of flow velocity. It is observable that when speed increases, the reliance of friction factor on Al_2O_3 concentration diminishes.

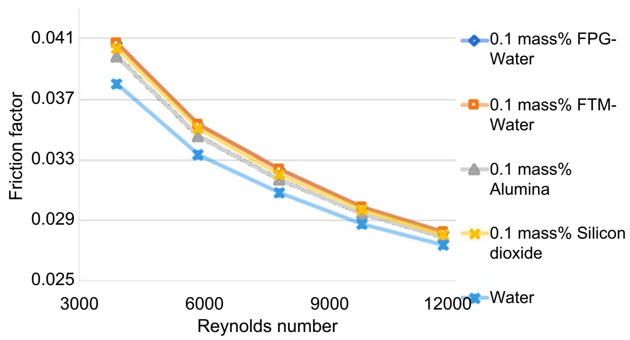

Fig. 16 Friction factor of tested nanofluids in 4-mm-diameter test rig at various velocities and input power of 23,870 W m^{-2}

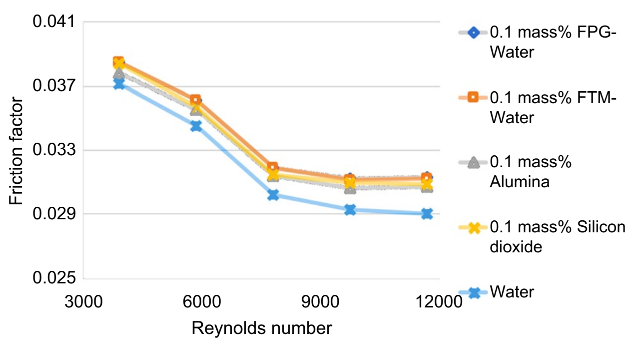

Fig. 17 Friction factor of tested nanofluids in 15-mm-diameter test section at dissimilar velocities and input power of 23,870 W m^{-2}

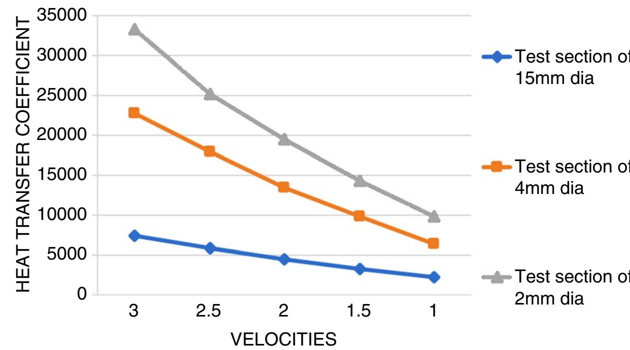

Fig. 18 Convective heat transfer coefficient of FPG-Water nanofluids in all test sections (2 mm, 4 mm and 15 mm diameters) of the test rig at inlet temperature of 30 °C at input power of 23,870 W m^{-2}

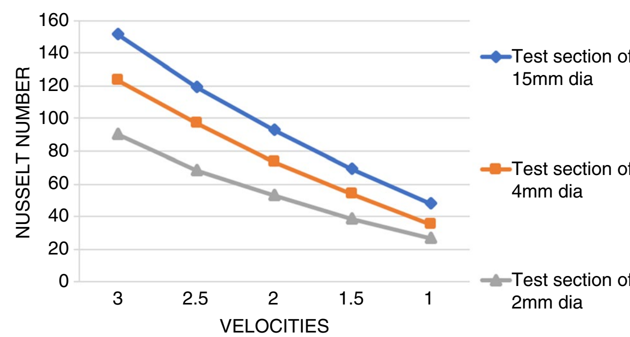

Fig. 19 Enhancement in Nusselt constant of tested FPG-Water nanofluid in all test sections (2 mm, 4 mm and 15 mm diameters) of the test rig at various velocities with input power of 23,870 W m^{-2}

To examine the size effect of using nanofluids, among all tested nanofluids FPG-Water nanofluid was selected (which has the highest heat transfer coefficient) to investigate the heat transfer enhancement. It was observed that by increasing the test section tube from 2 to 4 mm the heat transfer coefficient decreased up to 17% as shown in Fig. 18. Similarly same pattern was found in decrement of Nusselt number by increasing the size of test section. Therefore, Nusselt number decreased 18.4% in 4-mm-diameter test section compared to 2 mm test section (see Fig. 19). This may be attributed to lower test section diameter increasing rotational forces which causes thermal and velocity boundary layer to split, raising the Nusselt number. Moreover, to identify the heat transfer phenomena in 15 mm test section, it was compared with 2 mm test section diameter. It was observed that by increasing the test section diameter heat transfer properties decreased significantly. Therefore, in 15 mm test section diameter by using FPG-Water nanofluid the enhanced heat transfer coefficient was achieved up to 91.7% which is less than 24.7% in 2-mm-diameter test section (see Fig. 18). Also 33% decrease in Nusselt number was observed by using 15 mm test section in diameter as compared to test section of 2 mm in diameter (see Fig. 19). Similarly, friction factor also showed the significant change in pressure drop. By comparing the test sections of 2 mm and 4 mm diameter, it was found that 21% drop in friction factor was observed. Similarly, by comparing the test section of 2 mm and 15 mm diameter the change in friction loss was examined up to 21% decrease (see Fig. 20). This phenomenon could be observed that as test section size was increased the heat transfer as well as in friction factor showed significant decrease. This could be due to the change in surface area, and at the same time, constant heat flux was used in all three test sections. This occurrence is related to the idea of flow velocity and its effect on convective heat transfer. As fluid flows through a smaller diameter tube, it tends to involvement in a higher flow velocities compared to flowing through a larger diameter tube for the same flow rate. Higher flow velocities/Reynolds numbers lead to enhanced turbulence and mixing of the fluid. Turbulence increases the convective heart transfer operation by encourage superior mixing of the fluid and decreasing the emergence of stagnant boundary layers. The relationship between heat transfer coefficient and diameter is not globally true for all situations, but it can be a general observation in cases where flow velocity and turbulence are important factors. However, all four prepared nanofluids were used in all three test sections and the pattern was same in decrement of heat transfer values and friction factor by increasing the diameter of the test sections. Therefore, from Figs. 18–20 for the size comparison of different test sections we selected FPG-Water nanofluids which has a highest heat transfer coefficient in all test sections compared to base fluid. However, it was noticed that in this discussion Figs. 18–20 depict the trend of the absolute values of every parameter observed (h, Nu, friction factor) as a function of diameter for every fluid. By having this, we can clearly observe that not all parameter increase or decrease with the diameter of test section of the test rig.

When Reynolds numbers are small, Brownian motion may become the most important factor in regulating the rate at which nanoparticles and particles of the base liquid exchange momentum. Thus, when the Brownian motion increases, the friction factor increases with a steeper slope for all nanofluid types relative to the base fluid [39–43]. However, when Re levels are high, this mechanism is not dominating. In conclusion, the velocity of the working fluid is the most critical consideration in raising the friction constant at large Re. Generally, the little variance in rubbing factors between base fluid, metal oxide and functionalized nanofluid mixtures at various rates of volume flow can be ascribed to the small difference in viscosities between base fluids and nanofluids. The friction element varies due to the nanofluids' viscous drag effects. Therefore, the density of nanoparticles is a critical component in enhancing the

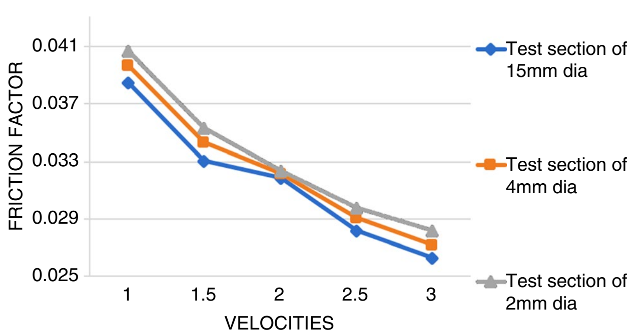

Fig. 20 Friction factor of FPG water nanofluids in all test sections (2 mm, 4 mm and 15 mm diameters) of the test rig at various velocities of 1–3 m s^{-1} and input power of 23,870 W m^{-2}

frictional properties of nanofluids. Pressure loss in the flow regime is related to the fluid's viscosity. This increased viscosity has a detrimental effect on pumping power. To ensure energy efficacy and minimize pumping power while effectively heating, it is crucial to construct a heat exchanger that is optimized for the application. However, in the process of measuring the effectiveness of nanofluids in different heat applications, it is important to avoid making significant mistakes. Table 6 presents a summary of the Nusselt number, friction factor and heat transfer coefficient for the tested nanofluids in various areas [36, 37].

Determining the effectiveness of nanofluids and base fluids is more critical than relying solely on heat transfer estimates. This is because the effectiveness of the nanofluid indicates whether it can replace the base fluid in a given application. Therefore, it is essential to evaluate the effectiveness of the nanofluid relative to the base fluid to determine its suitability for the intended application. Heat transfer estimate is a critical factor in heat transfer/pump power calculations. This enhancement comes from the thermal performance of nanofluids. The friction factor of lowest diameter test section of 2 mm diameter was lower compared to 4 mm and 15 mm test section as shown Table 6. Meanwhile, the heat transfer coefficient and Nusselt number was maximum in lowest diameter of test section. It was observed that while running the experiment at constant velocity the small size test section is completely filled with nanofluids because of that heat conduction is more than higher diameter test section. Therefore enhancement in thermal properties is higher than in lower diameter test section. After conducting tests on the 2-mm- and 4-mm-diameter test sections, it was found that the heat transfer coefficient for FPG-Water, FTM-Water, Al_2O_3 and SiO_2 increased by 15.72%, 16.4%, 5.75% and 3.45%, respectively, in the 2 mm test section. Furthermore, the heat transfer coefficient for these same nanofluids was significantly greater in the 15 mm test section, with increases of 25%, 23.83%, 7.95% and 8.23%, respectively, when compared to the 2 mm test section. These findings can be found in Table 6. However, Table 7 depicts the comparisons of previous studies in heat transfer enhancement with the present work.

Table 6 Summary of the heat transfer coefficient, Nusselt number and friction constant of selected nanofluids measured in different test sections

Nanofluids	Diameter 2 mm			Diameter 4 mm			Diameter 15 mm		
	HTC/%	Nu/%	FF/%	HTC/%	Nu/%	FF/%	HTC/%	Nu/%	FF/%
FPG-Water	116.4	79	5.53	100.68	66.7	7	91.7	59.3	7.61
FTM-Water	109.7	74	5.53	93.25	60.6	6.9	85.87	54.4	7.60
Al_2O_3	32.2	26.4	3.87	26.45	23.4	4.74	24.25	21.3	5.91
SiO_2	34.6	26.7	5.33	31.15	25	6.15	26.37	22.9	6.70

Table 7 Comparison of the present work with recent experimental studies in heat transfer performance of nanofluids

Nanomaterials	Base fluid	Observation	Investigator
Nitrogen-doped graphene (NDG) concentration of 0.06mass%	Water	The average increase in heat transfer coefficient was 16.2%. Nu increased up to 15.6%	Marjan et al. [44]
Graphene nanofluids with concentration of 0.1 vol%[	DI Water	Experimental investigations showed 33% increase in the Nu number produced by pulsed discharge method	Kotaro et al. [45]
Graphene/R141b nanofluids with concentration of 0.1mass%	Water	75% enhancement in heat transfer coefficient was achieved	Jianyang et al. [46]
Graphene nanoplatelets and multiwalled carbon nanotubes in the ratio of 1:1 with concentrations of 0.1 vol%	Water	Convective heat transfer coefficient was enhanced by 85% and Reynolds number remained constant	Balaji et al. [47]
Alumina nanofluids with concentrations of 0.01 to 0.2 vol%	DI water with mixture of ethylene glycol (15% and 30%)	Increase in thermal conductivity was achieved up to 9.1% and enhancement in heat transfer coefficient was achieved up to 27%	Ajeeb et al. [48]
Functionalized graphene nanoplatelets, alumina and silicon dioxide nanofluids with concentration of 0.1mass%	DI water	Highest heat transfer coefficient up to 116.4% in FPG-Water at 0.1mass%. Moreover, Al2O3 and SiO2 nanofluids exhibited decent enrichment in the heat transferal coefficients of up to 32.2% and 34.6%	Present work

Conclusions

This study delved into the convective heat transfer and friction loss attributes of an intriguing set of materials, including water-based nanofluids infused with Al_2O_3 and SiO_2, along with FPG-Water and FTM-Water. The circular test sections of stainless steel grade 316 of different diameters (2mm, 4mm and 15mm) were used. The tests were carried out at Reynolds numbers ranging from 3,900 to 11,700, with a consistent wall heat flux of 23,870 W m^{-2}. To produce widely distributed FPG-Water- and FTM-Water-based nanofluids, an unique functionalization approach has been developed for the first time. Heat transfer properties were significantly improved in all of the produced nanofluids. For comparing the effect of test section size, the test section with lowest diameter showed highest heat transfer performance. The observations might lead to the following conclusions:

1. The thermal conductivity of various materials has been studied, and the results show significant increases in certain materials. The top performers include FPG-Water and FTM-Water, which demonstrated an impressive increase of 32% and 31% compared to base fluid. Additionally, Al_2O_3 and SiO_2 showed an increase in thermal conductivity of 7.4% and 9%, respectively, compared to base fluid.
2. FPG-Water and FTM-Water nanofluids at 0.1 mass% demonstrated a remarkable increase in heat transfer coefficient of up to 116.4% and 109.7% compared to base fluid, in a 2-mm-diameter test segment. Similarly, Al_2O_3 and SiO_2 nanofluids at 0.1mass% also showed an increase in heat transfer coefficient of up to 32.2% and 34.6% compared to base fluid, respectively.
3. The thermal conductivity of FPG-Water, FTM-Water, Al_2O_3 and SiO_2 water-based nanofluids in a 2-mm-diameter test section was observed to be significantly higher compared to a 4mm and 15mm test section, with enhancements of up to 15.72%, 16.45%, 5.75% and 3.45%, and 24.7%, 23.83%, 7.95% and 8.23%, respectively.
4. The outcomes indicate that FPG-Water, FTM-Water, Al_2O_3 and SiO_2 at 0.1mass% can significantly enhance the Nusselt number. Specifically, by comparing with base fluid these nanofluids were found to increase the Nusselt number by up to 79%, 74%, 26.4% and 26.7%, respectively.
5. When compared to the base fluid, the frictional efficiency of FPG-Water and FTM-Water nanofluids may be raised by up to 7.61%. Al_2O_3 and SiO_2 nanofluids, on the other hand, might reach increases of up to 6.70%. As a result, substantial heat transfer enhancement might be accomplished at the expense of a little increase in frictional pressure drop.

The measured thermo-physical properties of whole nanofluids exhibited sensible performance necessary for a good heat exchanging liquid. Novel functionalization method is achieved to develop the graphene-based nanofluids and also achieved the significantly enhanced heat transfer properties.

Supplementary Information The online version contains supplementary material available at https://doi.org/10.1007/s10973-023-12595-2.

Acknowledgements The University of Malaya's Faculty of Engineering, Kuala Lumpur, Malaysia, provided the authors with the Intensive Research Grant UM. K/636/1/HIR (MOHE)/ENG45 and the UMRG Grant RP012A-13AET in exchange for their assistance in carrying out this study.

Authors contribution K.H.S. conducted the experiment, T.A.L. wrote the research article, I.A.M. carried out the data analysis, A.A.A. prepared the materials, and S.N.K. finalized the paper and validated the experiment.

References

1. Minakov AV, Guzei DV, Pryazhnikov MI, Zhigarev VA, Rudyak YY. Study of turbulent heat transfer of the nanofluids in a cylindrical channel. Int J Heat Mass Transf. 2016;102:745–55.
2. Babita SK, Sharma S, Gupta SM. Preparation and evaluation of stable nanofluids for heat transfer application: a review. Exp Thermal Fluid Sci. 2016;79:202–12.
3. Sadeghinezhad E, Mehrali M, Saidur R, Mehrali M, Tahan Latibari S, Akhiani AR, Metselaar HSC. A comprehensive review on graphene nanofluids: recent research, development and applications. Energy Convers Manag. 2016;111:466–87.
4. Solangi KH, Amiri A, Luhur MR, Akbari Ghavimi SA, Kazi SN, Badarudin A, Mohd Zubir MN. Experimental investigation of heat transfer performance and frictional loss of functionalized GNP-based water coolant in a closed conduit flow. RSC Adv. 2016;6(6):4552–63.
5. Strandberg R, Das DK. Finned tube performance evaluation with nanofluids and conventional heat transfer fluids. Int J Therm Sci. 2010;49(3):580–8.
6. Raja M, Vijayan R, Dineshkumar P, Venkatesan M. Review on nanofluids characterization, heat transfer characteristics and applications. Renew Sustain Energy Rev. 2016;64:163–73.
7. Haridas D, Rajput NS, Srivastava A. Interferometric study of heat transfer characteristics of Al_2O_3 and SiO_2-based dilute nanofluids under simultaneously developing flow regime in compact channels. Int J Heat Mass Transf. 2015;88:713–27.
8. Hussien AA, Abdullah MZ, Al-Nimr MDA. Single-phase heat transfer enhancement in micro/minichannels using nanofluids: theory and applications. Appl Energy. 2016;164:733–55.
9. Meybodi MK, Daryasafar A, Koochi MM, Moghadasi J, Meybodi RB, Ghahfarokhi AK. A novel correlation approach for viscosity prediction of water based nanofluids of Al_2O_3, TiO_2, SiO_2 and CuO. J Taiwan Inst Chem Eng. 2016;58:19–27.
10. Mostafizur RM, Abdul Aziz AR, Saidur R, Bhuiyan MHU. Investigation on stability and viscosity of SiO_2–CH_3OH (methanol) nanofluids. Int Commun Heat Mass Transfer. 2016;72:16–22.
11. Shahrul IMU, Mahbubul IM, Saidur R, Sabri MFM. Experimental investigation on Al_2O_3–W, SiO_2–W and ZnO–W nanofluids and their application in a shell and tube heat exchanger. Int J Heat Mass Transf. 2016;97:547–58.
12. Zhai YL, Xia GD, Liu XF, Li YF. Heat transfer enhancement of Al_2O_3-H_2O nanofluids flowing through a micro heat sink with complex structure. Int Commun Heat Mass Transfer. 2015;66:158–66.
13. Zhao N, Yang J, Li H, Zhang Z, Li S. Numerical investigations of laminar heat transfer and flow performance of Al_2O_3–water nanofluids in a flat tube. Int J Heat Mass Transf. 2016;92:268–82.
14. Zhao N, Yang J, Li S, Wang Q. Numerical investigation of laminar thermal-hydraulic performance of Al_2O_3–water nanofluids in offset strip fins channel. Int Commun Heat Mass Transfer. 2016;75:42–51.
15. Masuda H, Ebata A, Teramae K, Hishinuma N. Alteration of thermal conductivity and viscosity of liquid by dispersing ultra-fine particles (dispersion of-Al_2O_3, SiO_2 and TiO_2 ultra-fine particles). Netsu Bussei. 1993;4(4):227–33.
16. Younghwan KK, Cho Y, Li C, Cheong C, Hwang Y. Convective heat transfer characteristics of nanofluids under laminar and turbulent flow conditions. Curr Appl Phys. 2009;9:63.
17. Abdolbaqi MK, Sidik NAC, Rahim MFA, Mamat R, Azmi WH, Yazid MNAWM, Najafi G. Experimental investigation and development of new correlation for thermal conductivity and viscosity of BioGlycol/water based SiO_2 nanofluids. Int Commun Heat Mass Transf. 2016;77:54–63.
18. Solangi KH, Kazi SN, Luhur MR, Badarudin A, Amiri A, Sadri R, Zubir MNM, Gharehkhani S, Teng KH. A comprehensive review of thermo-physical properties and convective heat transfer to nanofluids. Energy. 2015;89:1065–86.
19. Minea AA. Hybrid nanofluids based on Al_2O_3, TiO_2 and SiO_2: Numerical evaluation of different approaches. Int J Heat Mass Transf. 2017;104:852–60.
20. Pak BC, Cho YI. Hydrodynamic and heat transfer study of dispersed fluids with submicron metallic oxide particles. Exp Heat Transfer. 1998;11:151–70.
21. Wen D, Ding Y. Experimental investigation into convective heat transfer of nanofluids at the entrance region under laminar flow conditions. Int J Heat Mass Transf. 2004;47(24):5181–8.
22. Sharma KV, Sundar LS, Sarma PK. Estimation of heat transfer coefficient and friction factor in the transition flow with low volume concentration of Al_2O_3 nanofluid flowing in a circular tube and with twisted tape insert. Int Commun Heat Mass Transfer. 2009;36(5):503–7.
23. Ferrouillat S, Bontemps A, Ribeiro JP, Gruss JA, Soriano O. Hydraulic and heat transfer study of SiO_2/water nanofluids in horizontal tubes with imposed wall temperature boundary conditions. Int J Heat Fluid Flow. 2011;32(2):424–39.
24. Yarmand H, Gharehkhani S, Shirazi SFS, Amiri A, Alehashem MS, Dahari M, Kazi SN. Experimental investigation of thermo-physical properties, convective heat transfer and pressure drop of functionalized graphene nanoplatelets aqueous nanofluid in a square heated pipe. Energy Convers Manag. 2016;114:38–49.
25. Zubir MNM, Badarudin A, Kazi SN, Misran M, Amiri A, Sadri R, Khalid S. Experimental investigation on the use of highly charged nanoparticles to improve the stability of weakly charged colloidal system. J Colloid Interface Sci. 2015;454:245–55.
26. Ali AGS, Ebrahimzadeh MH, Shokrgozar MA, Solati-Hashjin M, Abu ONA. Effect of starch content on the biodegradation of polycaprolactone/starch composite for fabricating in situ pore-forming scaffolds. Polym Testing. 2015;43:94–102.
27. Amiri A, Shanbedi M, Chew BT, Kazi SN, Solangi SK. Toward improved engine performance with crumpled nitrogen-doped graphene based water–ethylene glycol coolant. Chem Eng J. 2016;289:583–95.
28. Solangi KH, Amiri A, Luhur MR, Ghavimi SAA, Zubir MNM, Kazi SN, Badarudin A. Experimental investigation of the propylene glycol-treated graphene nanoplatelets for the enhancement of closed conduit turbulent convective heat transfer. Int Commun Heat Mass Transfer. 2016;73:43–53.
29. Selvam C, Balaji T, Mohan Lal D, Harish S. Convective heat transfer coefficient and pressure drop of water-ethylene glycol

mixture with graphene nanoplatelets. Exp Thermal Fluid Sci. 2017;80:67–76.

30. Mehrali M, Sadeghinezhad E, Rosen MA, Tahan Latibari S, Mehrali M, Metselaar HSC, Kazi SN. Effect of specific surface area on convective heat transfer of graphene nanoplatelet aqueous nanofluids. Exp Thermal Fluid Sci. 2015;68:100–8.
31. Sadeghinezhad E, Togun H, Mehrali M, Sadeghi NejadC P, Tahan Latibari T, Abdulrazzaq T, Kazi SN, Metselaar HSC. An experimental and numerical investigation of heat transfer enhancement for graphene nanoplatelets nanofluids in turbulent flow conditions. Int J Heat Mass Transf. 2015;81:41–51.
32. Sundaram P, Kalaisselvane A, Sathishkumar A, Ganesh KP, Chul KS, Prabakaran R. Synthesis, stability, and heat transfer behavior of water and graphene nanoplatelet-based nanofluid for cool thermal storage applications. J Energy Storage. 2023. https://doi.org/10.1016/j.est.2023.107219.
33. Sebastian D, Tiew WT, Brigitte V. Comparison of heat transfer performance of water-based graphene nanoplatelet- and multiwalled carbon nanotube-nanofluids in a concentric tube heat exchanger. Diamond Related Mater. 2022. https://doi.org/10.1016/j.diamond.2022.108976.
34. Esmaeilzadeh N, Nik-Ghazali HSC, Metselaar MS, Naghavi M, Azuddin S, Iranmanesh S. Thermal performance evaluation of the heat pipe by using 1-pyrene carboxylic-acid functionalized graphene nanofluid. Int Commun Heat Mass Transf. 2021;6:129. https://doi.org/10.1016/j.icheatmasstransfer.2021.105669.
35. Chenlei Q, Jieqing Z, Shaoyu W, Ruoyu D, Jinhao Z. Multiobjective optimisation of thermal and hydraulic performance with various concentrations of hybrid Fe_3O_4/graphene nanofluids in a microchannel heat sink. Case Stud Therm Eng. 2023;45:69.
36. Decagon Devices, Inc. 2365 NE Hopkins Court Pullman WA 99163. https://library.metergroup.com/Manuals/13351_KD2%20Pro_Web.pdf
37. Keen innovative soluitions, Techno 2-ro, Yuseong-gu, Daejeon, Republic of Korea. URL: https://klabkis.com/english/0201_Alpha?gclid=CjwKCAjwoqGnBhAcEiwAwK-OkUOqBLC-QZDxWZY7W3DUbNP6f68A2hLyXfP6xcPlBet78EKn0YTiixoC62IQAvD_BwE
38. Vandsburger L. Synthesis and Covalent Surface Modification of Carbon Nanotubes for Preparation of Stabilized Nanofluid Suspensions. McGill University, 2009.
39. Shanbedi M, Amiri A, Rashidi S, Heris SZ, Baniadam M. Thermal performance prediction of two-phase closed thermosyphon using adaptive neuro-fuzzy inference system. Heat Transfer Eng. 2015;36(3):315–24.
40. Shanbedi M, Heris SZ, Baniadam M, Amiri A, Maghrebi M. Investigation of heat-transfer characterization of EDA-MWCNT/DI-water nanofluid in a two-phase closed thermosyphon. Ind Engg Chem Research. 2012;51(3):1423–8.
41. Aboraia AM, Hamdalla TA, Darwish Alotaibi BM, Al-Ghamdi SA, Alfadhli S, Mohamed S. Synthesis, the structural and thermal stability of $LiCo_{1-x}Fe_xPO_4$. J Therm Anal Calorim. 2023. https://doi.org/10.1007/s10973-023-12030-6.
42. Majedi SA, Azizi S, Peyghambarzadeh B. Investigation and measurement of crude oil heat transfer coefficient in forced convection and subcooled flow boiling heat transfer. J Therm Anal Calorim. 2023. https://doi.org/10.1007/s10973-023-12065-9.
43. Sonawane C, Praharaj P, Kulkarni K. Numerical simulation of heat transfer characteristics of circular cylinder forced to oscillate elliptically in an incompressible fluid flow. J Therm Anal Calorim. 2023;148:2719–36. https://doi.org/10.1007/s10973-022-11621-z.
44. Marjan G, Kherbeet AS, Masoud A, Sadeghinezhad E, Mehrali M, Zahedi P, Somchai W, Dahari M. Investigation of heat transfer performance and friction factor of a counter-flow double-pipe heat exchanger using nitrogen-doped, graphene-based nanofluids. Int Commun Heat Mass Transfer. 2016;76:16–23.
45. Kotaro F, Shibata A, Torii S. An experimental and numerical study of turbulent heat transfer enhancement for graphene nanofluids produced by pulsed discharge. Int J Thermofluids. 2022;16:46.
46. Jianyang Z, Xiaoping L, Bolin H, Changzheng L, Lizhe L, Zhixin Y, Zhi QT. Comprehensive evaluation of graphene/R141b nanofluids enhanced heat transfer performance of minichannel heat sinks. Powder Technol. 2022;397:69317.
47. Balaji T, Sharan R, Selvam C, Mohan LD. Enhanced heat transfer characteristics of water based hybrid nanofluids with graphene nanoplatelets and multi walled carbon nanotubes. Powder Technol. 2021;394:526.
48. Ajeeb W, Renato RS, da Thieleke S, Murshed S. Experimental investigation of heat transfer performance of Al_2O_3 nanofluids in a compact plate heat exchanger. Appl Therm Eng. 2023;218:685.

Publisher's Note Springer Nature remains neutral with regard to jurisdictional claims in published maps and institutional affiliations.